SUPPLEMENTAL MATERIALS

FIGURES

TABLES

MOVIES

Figure S1

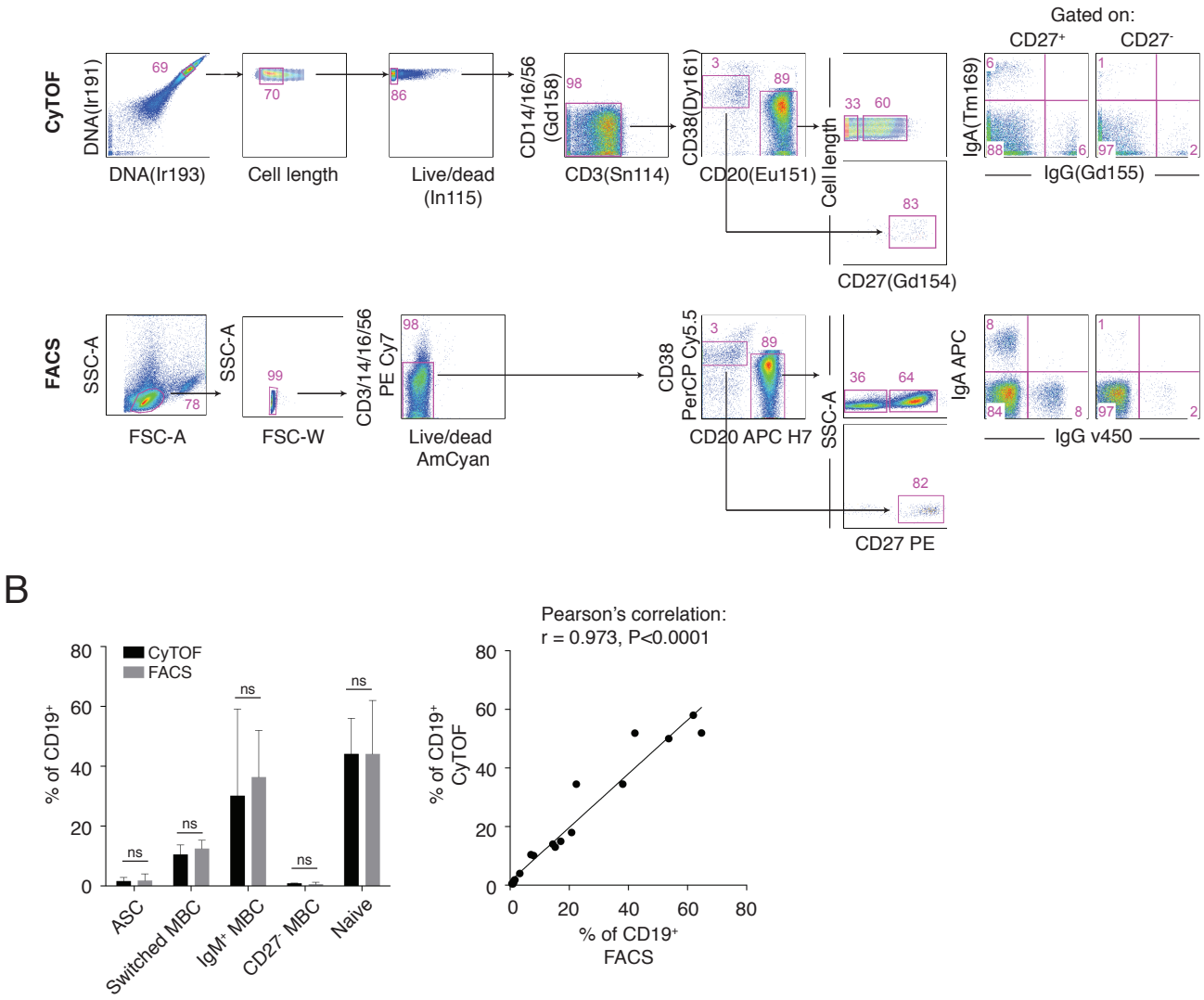

Figure S1. Direct comparison of mass cytometry and flow cytometry gating strategies to identify human B cell subsets. (A) Three million enriched peripheral blood B cells from the same donor were stained in parallel with metal-tagged (**Table S1**) or fluorescently labeled antibody panels for analysis by mass cytometry or flow cytometry, respectively. Shown are representative 2D mass cytometry and flow cytometry dot plots (100,000 events acquired per sample) from a single donor depicting the gating strategy used and the frequencies of subsets as determined by CyTOF and FACS. **(B)** Bar graphs (left) represent the median frequencies ± range of ASCs, switched MBCs, IgM$^+$ MBCs, CD27$^-$ MBCs, and naïve B cells among CD19$^+$ cells as determined by mass cytometry or flow cytometry (four donors). ns, P>0.5; unpaired t-test. Correlation (right) between frequencies of B cell subsets as determined by mass cytometry versus flow cytometry. Pearson's correlation coefficient is displayed.

Figure S2

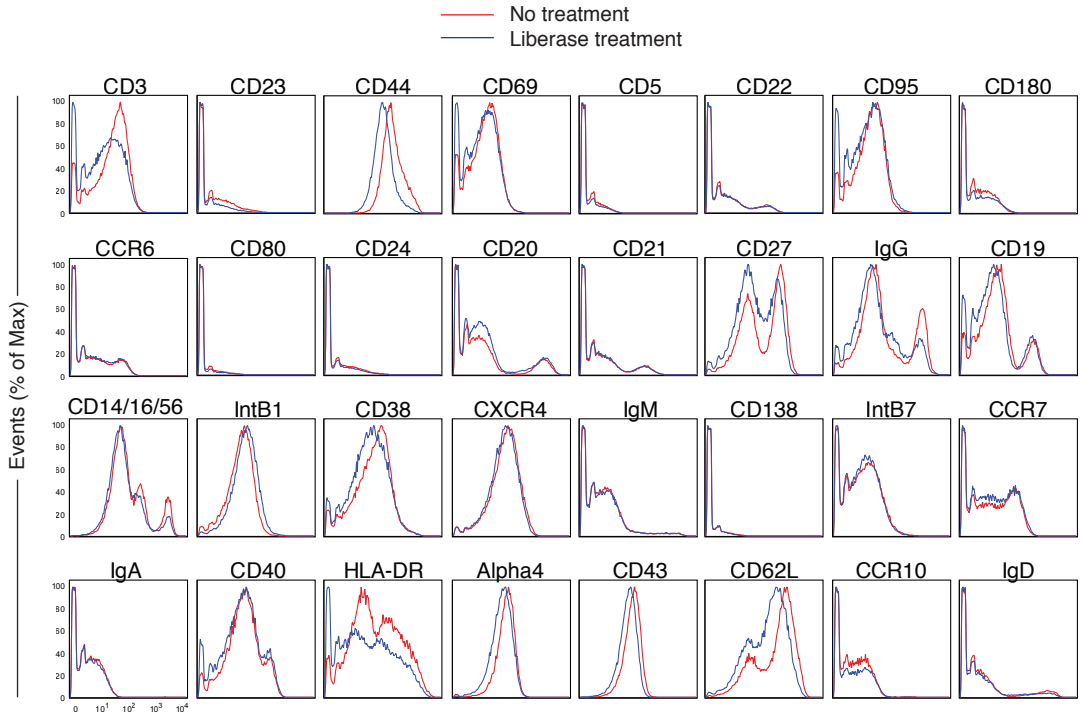

Figure S2. Comparable cell surface expression of markers included in mass cytometry antibody panel on PBMCs with and without liberase treatment. Five million peripheral blood mononuclear cells from a healthy donor were enzymatically treated with liberase for 1 hr at 37 ºC. Cells were washed with complete RPMI and rested for 2 h at 37 ºC and 5% CO_2 prior to mass cytometry staining with the metal-tagged antibody panel listed in Table S1. Shown are mass cytometry histogram overlays of the expression of each cell surface marker on total PBMCs with and without liberase treatment. At least 100, 000 events were acquired per sample.

Figure S3

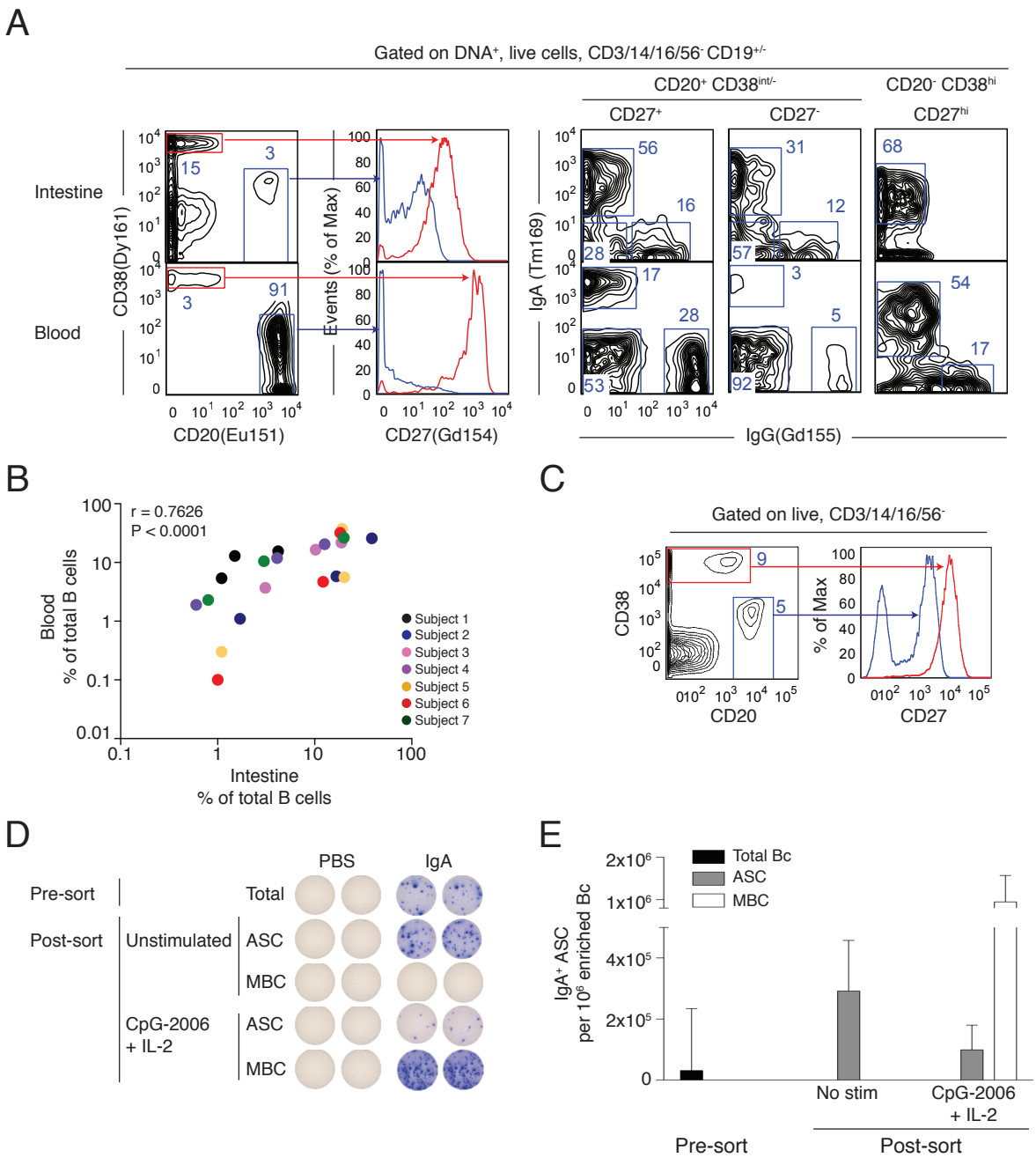

Figure S3. Identification and functional characterization of ASCs and non-ASCs in the intestine and blood. (A) Representative 2D mass cytometry plots showing the gating strategy used to identify ASCs ($CD20^{lo/-}CD27^{hi}CD38^{hi}$), switched MBCs ($CD20^{+}CD27^{+}CD38^{int/-}$IgG/$IgA^{+}$), $CD27^{-}$ MBCs ($CD20^{+}CD27^{-}CD38^{int/-}$IgG/$IgA^{+}$), IgM^{+} MBCs ($CD20^{+}CD27^{+}CD38^{int/-}$IgG/$IgA^{-}$) and naive B cells ($CD20^{+}CD27^{-}CD38^{int/-}$IgG/$IgA^{-}$) **(B)** Correlation of the frequency of switched MBCs, IgM^{+} MBCs and $CD27^{-}$ MBCs in the intestine and the blood of the same donors. Dots represent MBC subsets. Colors represent each donor analyzed. Spearman's correlation coefficient is shown. **(C)** Intestinal ASCs and MBCs were sorted for analysis by Elispot. Shown are representative flow cytometry plots from a single donor. **(D)** The frequency of IgA^{+} ASCs among sorted total intestinal ASCs and MBCs was determined by Elispot. Sorted ASCs and MBCs were stimulated for 5 days with CpG-2006 and IL-6 *in vitro* and the frequency of IgA^{+} ASC was determined post stimulation. Shown is a representative Elispot detection of total IgA^{+} ASCs among pre-sorted intestinal B cells or sorted intestinal ASCs and MBCs. **(E)** Bar graph of the median frequencies ± range of total IgA^{+} ASCs in enriched intestinal B cells prior to and following sorting, with or without polyclonal stimulation, in three donors.

Figure S4

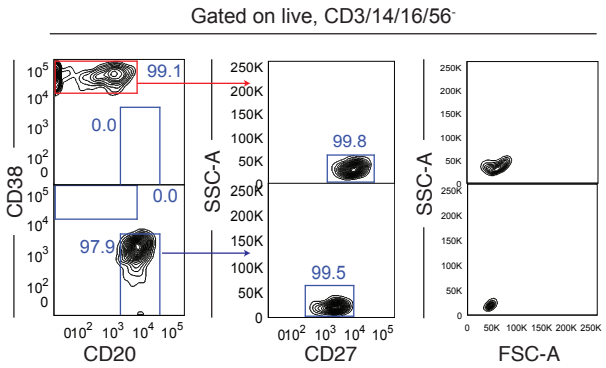

Figure S4. Purity of FACS-sorted intestinal ASCs and MBCs used for Elispot and qRT-PCR. Shown are 2D contour plots from a representative donor demonstrating the purity (>97%) of FACS-sorted intestinal ASCs ($CD20^{lo/-}$ $CD27^{hi}$ $CD38^{hi}$ (large FSC x SSC)) and MBCs ($CD20^{+}$ $CD27^{+}$ $CD38^{int/-}$ (small FSC x SSC)) used for Elispot or qRT-PCR (**Table S2**). At least 1000 events were acquired per sample.

Figure S5

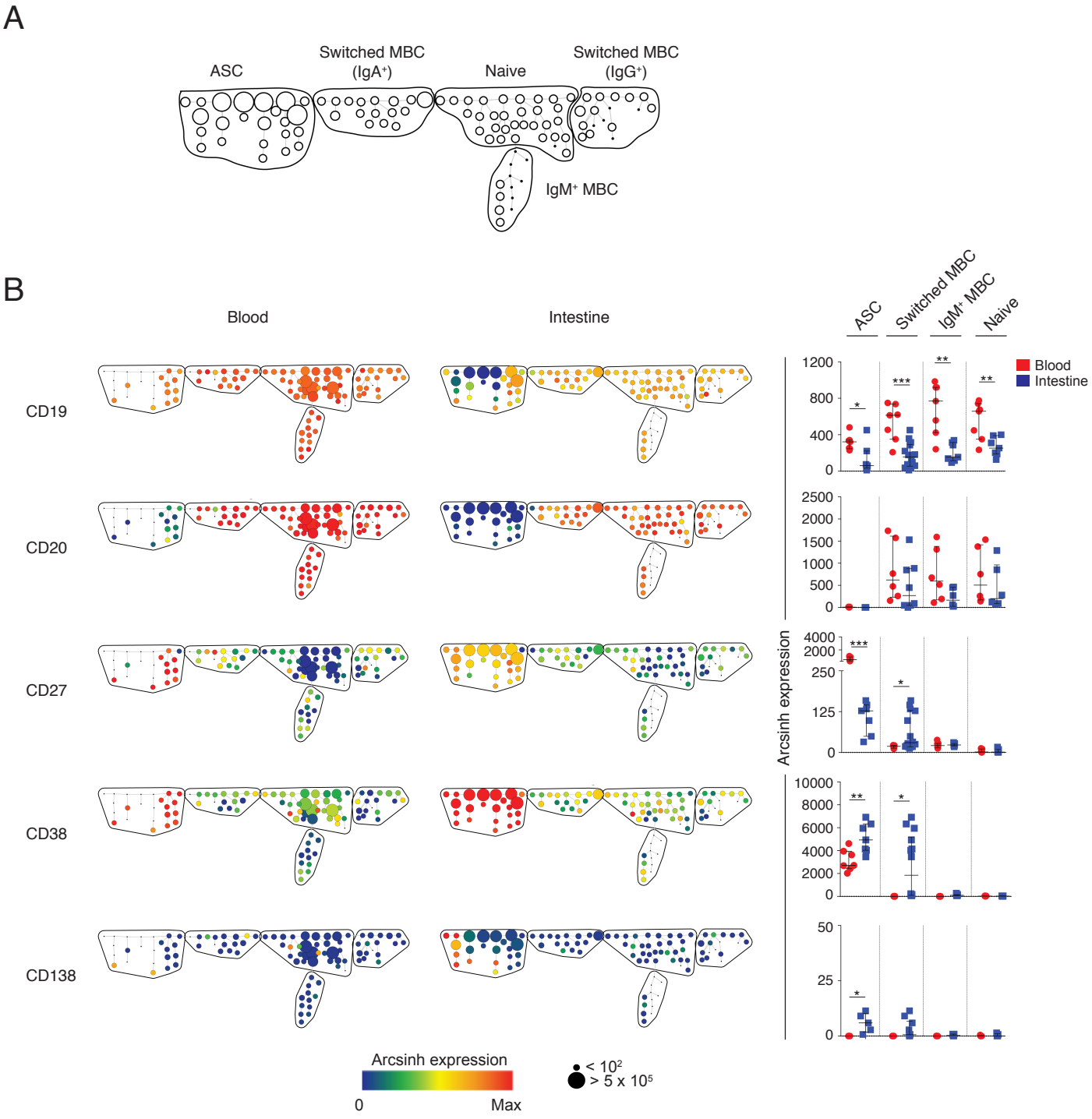
A
ASC
Switched MBC (IgA+)
Naive
Switched MBC (IgG+)
IgM+ MBC
B
Blood
Intestine
ASC
Switched MBC
IgM+ MBC
Naive
CD19
CD20
CD27
CD38
CD138
Blood
Intestine
Arcsinh expression
Arcsinh expression
0
Max
< 10²
> 5 x 10⁵

Figure S5 (cont)

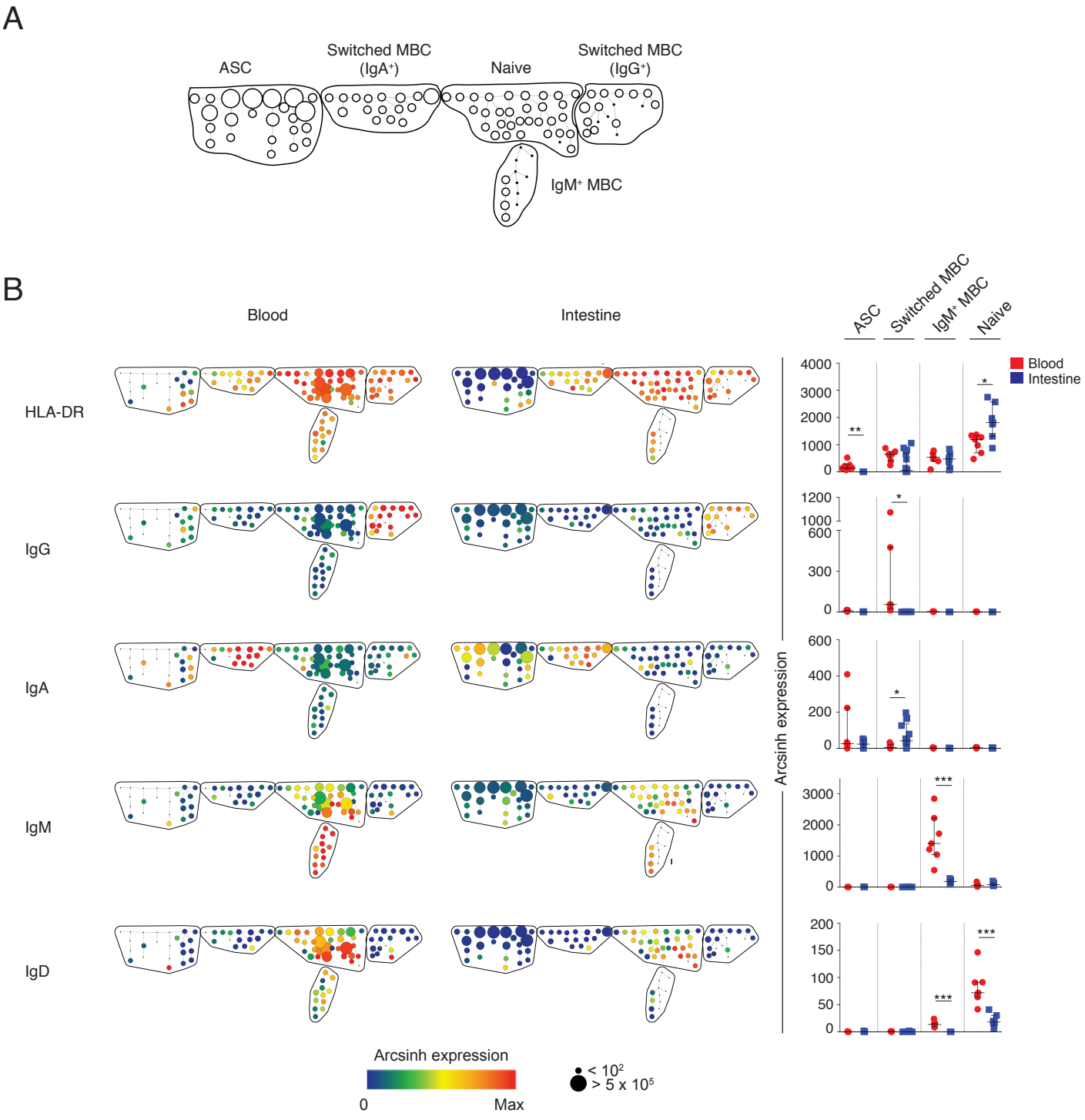

Figure S5. Expression of B cell lineage markers in intestinal and peripheral blood B cells used for clustering analysis by SPADE. (A) Skeleton structure of the SPADE tree for peripheral blood and intestinal B cells based on data from seven donors. **(B)** Representative SPADE tree from a single donor depicting the expression of all lineage markers in the blood and intestine. Node color represents arcsinh expression of marker indicated to the left of the tree according to the 5-point color scale below the tree, and size represents frequency as indicated in the scale. Dot plots (right) represent the median arcsinh expression ± range of each marker across B cell subsets in the peripheral blood and intestine of seven donors. *, P<0.05; **, P<0.005; ***, P<0.0005; unpaired t-test.

Figure S6

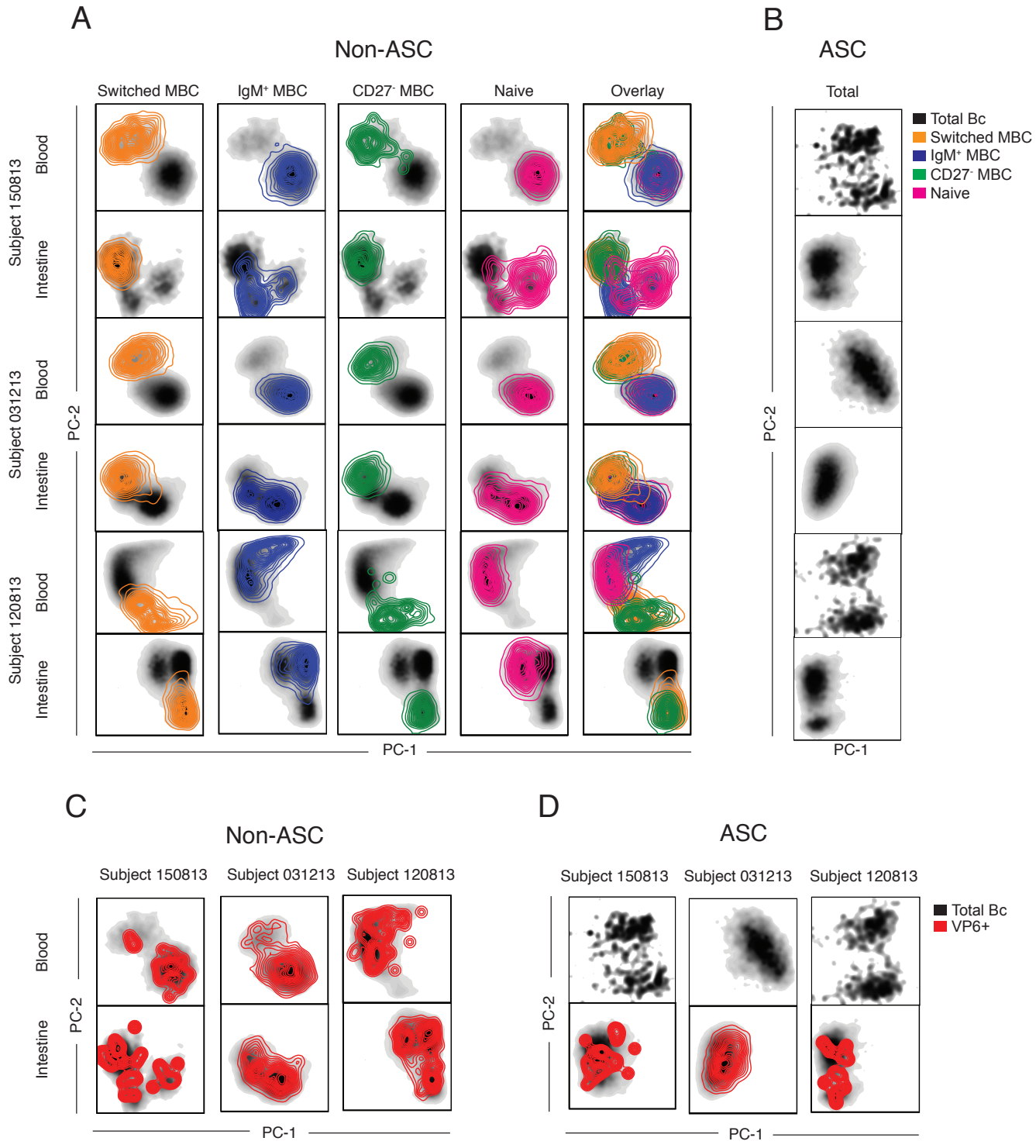
A
Non-ASC
Switched MBC
IgM+ MBC
CD27- MBC
Naive
Overlay
Subject 150813
Blood
Intestine
Subject 031213
Blood
Intestine
Subject 120813
Blood
Intestine
PC-2
PC-1
B
ASC
Total
Total Bc
Switched MBC
IgM+ MBC
CD27- MBC
Naive
PC-2
PC-1
C
Non-ASC
Subject 150813
Subject 031213
Subject 120813
Blood
Intestine
PC-2
PC-1
D
ASC
Subject 150813
Subject 031213
Subject 120813
Total Bc
VP6+
PC-2
PC-1

Figure S6 (cont)

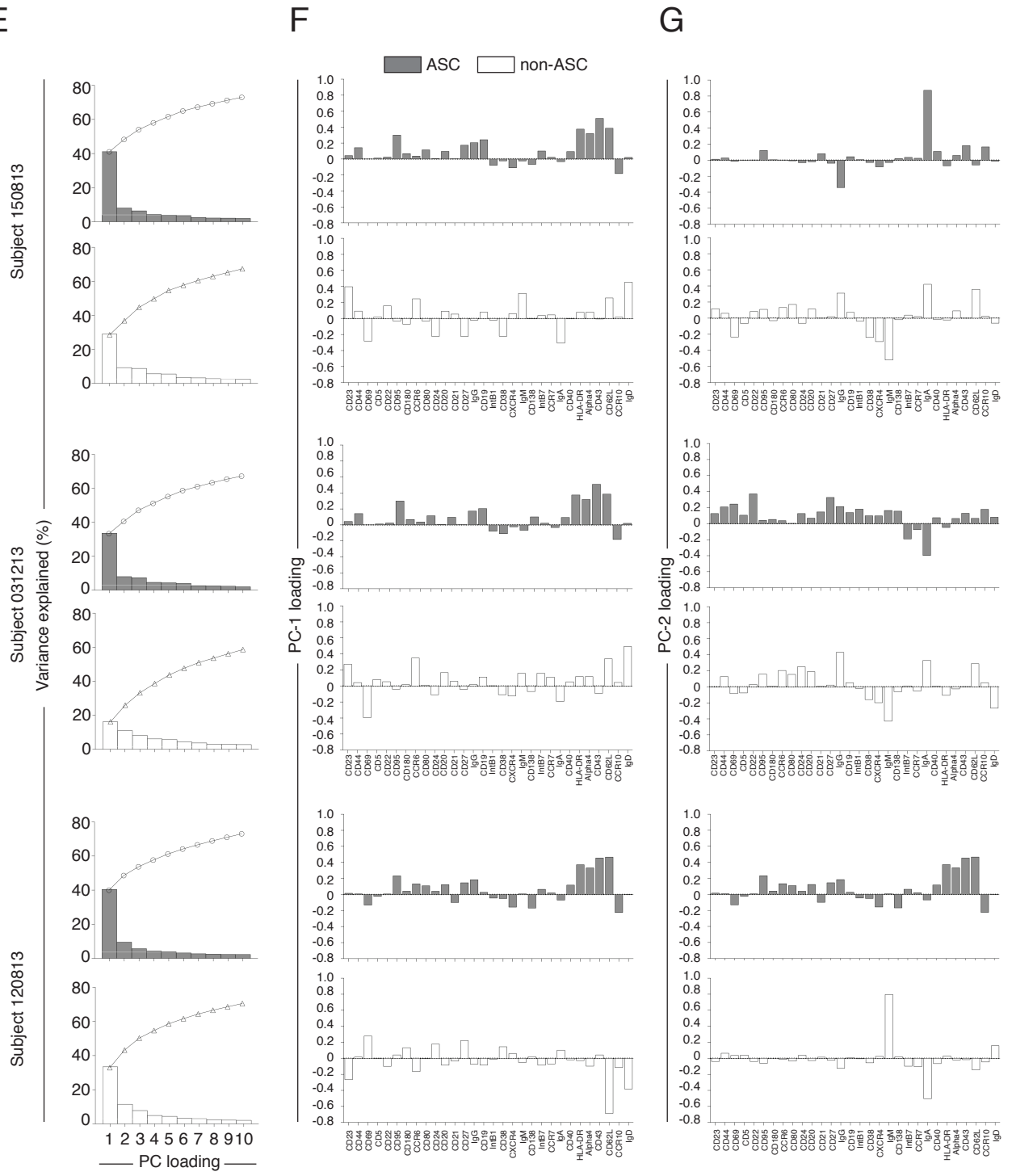

Figure S6. PCA reveals conserved relationships between B cell subsets and consistent VP6-binding reactivity mong different donors analyzed. Colored contour density plots of the first two principal components representing classically gated **(A)** switched MBCs, IgM⁺ MBCs, CD27⁻ MBCs, naïve B cells and **(B)** ASCs in the blood and intestine of three donors. VP6-specific **(C)** Non-ASCs and **(D)** ASCs are represented separately as red contour density plots. **(E)** The percent variation explained is plotted for each component (bars) and cumulatively (line) for ASC and non-ASC for the three subjects. **(F, G)** Principal component loading values (weighting coefficients) for the first two components for ASC and non-ASC subsets are plotted for each parameter of the analysis.

Figure S7

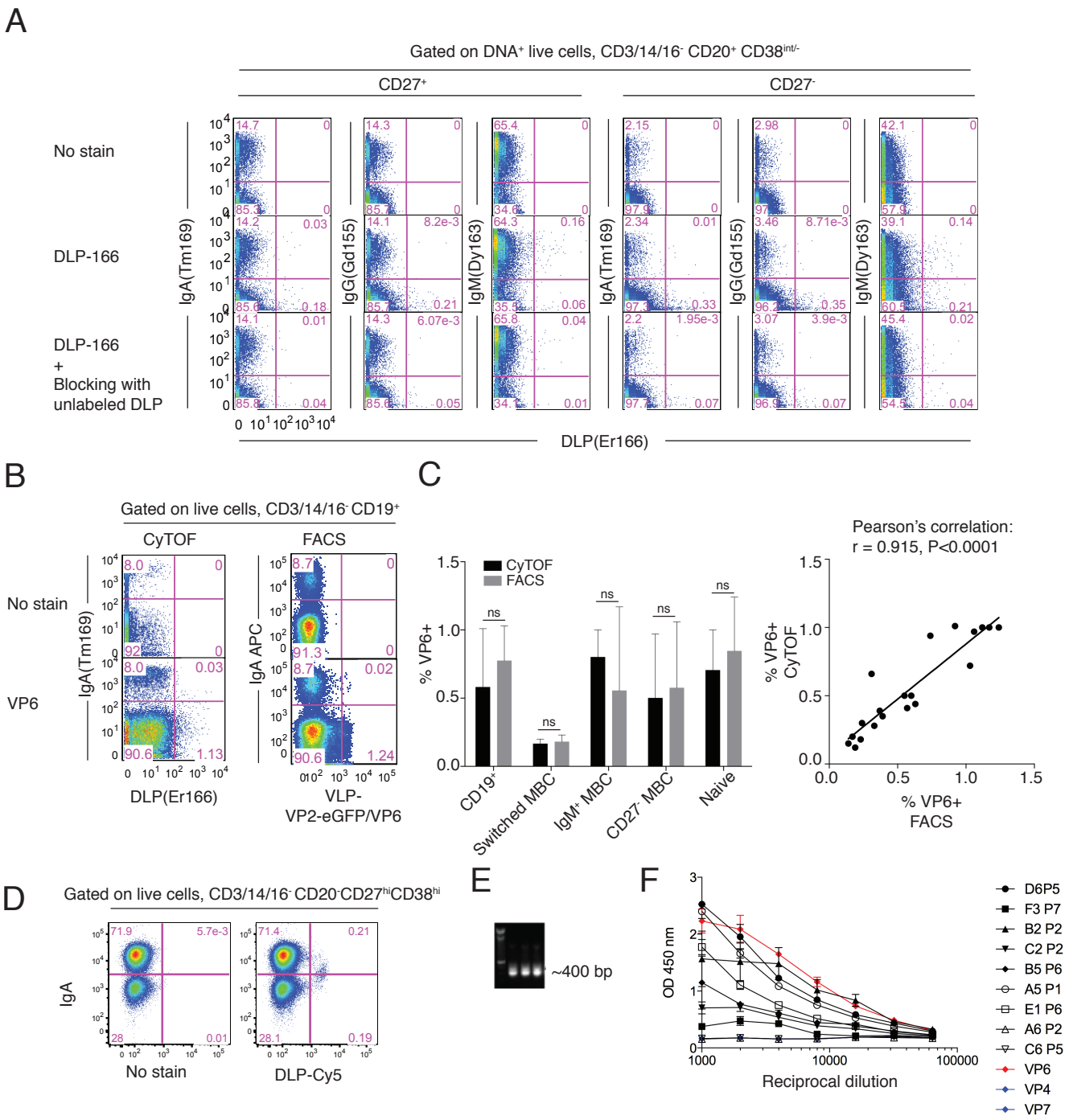

Figure S7. Validation of mass cytometry identification of VP6-specific human B cells. (A) Three million enriched peripheral blood B cells were stained with DLP-Er166 to identify VP6-binding B cell subsets (middle panel) by mass cytometry. Stringent gating of VP6-binding B cells was performed based on unstained controls (top panel). Specificity of VP6-specific B cell staining was demonstrated by blocking with unlabeled DLPs (bottom panel). Shown are representative 2D mass cytometry dot plots from a single donor. **(B)** Direct comparison of VP6-specific B cell identification by mass cytometry versus flow cytometry. Two million enriched peripheral blood B cells from the same subject were stained with either DLP-Er166 or VLPs expressing VP2-eGFP/VP6 for analysis by CyTOF or FACS, respectively. Shown are representative 2D mass cytometry and flow cytometry dot plots from a representative donor (100,000 events acquired per sample). **(C)** Bar graph of median frequencies ± range of VP6-specific B cells as determined by CyTOF or FACS in samples from four donors. ns, P>0.5; unpaired t-test. Correlation (right) is shown between frequencies of VP6-specific B cells as determined by mass cytometry versus flow cytometry. Pearson's correlation coefficient is displayed. **(D)** DLP-binding intestinal IgA+ ASC from gastric bypass patients were single-cell sorted into RNA lysis buffer and **(E)** IgH and IgLk V genes were amplified by RT-PCR and cloned into IgG expression vectors to express human mAbs. **(F)** Shown is the Elisa binding reactivity of 9 human mAbs (black), and mouse mAbs specific to VP6 (red), VP4 and VP7 (blue) to DLPs.

Table S1. Mass cytometry antibody panel for B cell phenotyping

Isotope	Antibody	Antibody Clone	Company
112Cd	CD3 qdot 655	S4.1	Invitrogen
115In	DOTA-maleimide		Macrocyclics, Inc.
139La	CD23	ML233	BD Pharmingen
141Pr	CD44	BJ18	Biolegend
142Nd	CD69	FN50	BD Biosciences
143Nd	CD5	UCH12	Biolegend
144Nd	CD22	HIB22	BD Biosciences
145Nd	CD95	DX2	BD Biosciences
146Nd	CD180	MHR73-11	BD Biosciences
147Sm	CCR6	11A9	BD Biosciences
149Sm	CD80	L307.4	BD Biosciences
150Sm	CD24	ML5	BD Biosciences
151Eu	CD20	2H7	BD Biosciences
153Eu	CD21	1048	BD Biosciences
154Gd	CD27	LG.7F9	eBiosciences
155Gd	IgG	G18-145	BD Biosciences
157Gd	CD19	H1B19	BD Biosciences
158Gd	CD14	M5E2	Biolegend
158Gd	CD16	3G8	BD Biosciences
158Gd	CD56	HCD56	Biolegend
160Gd	Integrin B1	MAR4	BD Biosciences
161Dy	CD38	HIT2	Biolegend
162Dy	CXCR4	12G5	Biolegend
163Dy	IgM	G20-127	BD Biosciences
165Ho	CD138	DL-101	BD Biosciences
166Er	DLP (RRV strain)		
167Er	Integrin B7	FIB504	Biolegend
168Er	CCR7	150503	R&D Systems
169Tm	IgA	G18-1	BD Biosciences
170Yb	CD40	5C3	BD Biosciences
171Tb	HLA-DR	L243	BD Biosciences
172Yb	Alpha 4	9F10	Biolegend
173Yb	CD43	84-3C1	eBioscience
174Yb	CD62L	DREG-56	BD Biosciences
175Lu	CCR10	1B5	Millenium Pharmaceuticals
176Yb	IgD	IA6-2	BD Biosciences

Table S2. Purity of FACS-sorted intestinal ASCs and MBCs used for Elispot and qRT-PCR. Intestinal ASCs and MBCs were sorted based on CD3/14/16/56^{-} CD20$^{lo/-}$CD27^{hi}CD38^{hi} and CD3/14/16/56^{-}CD20^{+}CD27^{+}CD38$^{int/-}$ phenotypes, respectively (**Fig. S3**). Shown is the median purity and range of sorted intestinal ASCs and MBCs from three donors used for Elispot or qRT-PCR. At least 1000 events were acquired per sample.

Sorted subset	Analysis	Median purity (range) (%)	N
Intestinal ASC	Elispot	>99.9 (96.9 - >99.9)	3
	qRT-PCR	99.0 (99.0 - >99.9)	3
Intestinal MBC	Elispot	98.0 (97.6 - 99.5)	3
	qRT-PCR	98.0 (96.0 - 99.1)	3

Table S3. V gene segment usage among VP6-specific intestinal ASCs isolated using DLP-Cy5

mAb	Donor	VH	JH	DH	VK	JK
A5	1	4-4	6	2-21	3-20	4
B2	1	4-4	6	3-3	1-9	5
C3	1	4-4	3	3-3	1-9	5
D6	1	4-39	2	3-22	3-20	4
B5	1	4-4	6	3-3	1-9	2
E1	1	4-4	6	2-21	3-20	3
F3	1	4-4	4	3-22	1-39	2

Movie S1. 3D PCA PyMOL visualization of the continuum of B cell differentiation in the intestine and the blood

Each dot represents a single cell and is plotted in 3D according to the first three principal components. The color of the dot represents a specific B cell subset: switched MBCs (orange), IgM+ MBCs (blue), CD27- MBCs (green) and naïve B cells (pink) from the (**A**) blood and (**B**) intestine of the donor represented in Fig. 5.